Spectrochimica Acta Part A: Molecular and Biomolecular Spectroscopy 273 (2022) 120979

Contents lists available at ScienceDirect

Spectrochimica Acta Part A: Molecular and Biomolecular Spectroscopy

journal homepage: www.elsevier.com/locate/saa

The behavior of zeolites wairakite and phillipsite at high *P-T* parameters

Ulyana Borodina [a,*], Sergey Goryainov [a], Svetlana Krylova [b], Alexander Vtyurin [b], Alexander Krylov [b]

[a] Sobolev Institute of Geology and Mineralogy, Siberian Branch of Russian Academy of Sciences, pr. Acad. Koptyug 3, 630090 Novosibirsk, Russia
[b] Kirensky Institute of Physics, Federal Research Center KSC SB RAS, Academgorodok 50/38, 660036 Krasnoyarsk, Russia

HIGHLIGHTS

- In Raman spectra breathing modes of single 4-membered aluminosilicate rings are the strongest.
- Up to T = 350 °C and P = 1.7 GPa phillipsite compressed in water retains the initial phase.
- Wairakite partially dissolve with further formation of phillipsite at T > 250 °C, P > 0.4 GPa.
- Besides phillipsite, we observe formation of unidentified phase X from wairakite-water system.

GRAPHICAL ABSTRACT

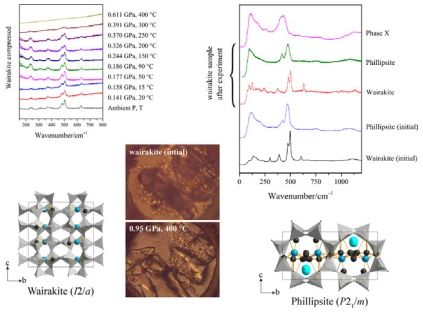

ARTICLE INFO

Article history:
Received 22 October 2021
Received in revised form 15 January 2022
Accepted 29 January 2022
Available online 2 February 2022

Keywords:
Wairakite
Phillipsite
Zeolites
Raman
High pressure
High temperature

ABSTRACT

In situ investigation of mineral behavior in water medium at simultaneously high *P-T* parameters can be applied to modelling of mineral transformation processes in lithospheric plates. The behavior of zeolites wairakite and phillipsite under the *P-T* conditions of «cold» slab subduction, corresponding to the start of oceanic plate diving or ocean floor near geothermal sources, was studied by *in situ* Raman spectroscopy. During compression in water medium, phillipsite initial phase is stable up to T = 350 °C, P = 1.7 GPa and with further increase of *P-T* parameters, phillipsite undergoes amorphization and partially dissolves in water. Wairakite compressed in water medium has a polymorphic transformation at $T \approx 300$ °C and $P \approx 0.4$ GPa. At 300–450 °C and P = 1 GPa the Raman spectrum almost disappears due to the amorphization of wairakite. Zeolite wairakite partially dissolves, and other zeolite phillipsite grows out of the fluid at T = 450 °C and P = 1 GPa. This transformation indicates the higher stability of phillipsite in comparison to wairakite. The *in situ* observed high *P-T* stability of phillipsite, which does not transform to other zeolites, and its formation from wairakite may indicate ϕ possible widespread distribution of this zeolite in marine sediments.

By using the plane-wave pseudo-potential method, ab initio DFT calculations of Raman and FTIR spectra of wairakite were carried out. Comparing theoretical and experimental spectra, interpretation of the vibrational spectra of both zeolites was suggested.

1. Introduction

Zeolites are natural crystalline aluminosilicates with a framework structures filled with water and exchangeable cations; ion exchange is possible at low temperature (100 °C at the most), and water is lost at about 250 °C and reversibly re-adsorbed at room temperature. The primarily building units of the structures are TO_4 tetrahedra, where T = Si, Al [1]. Zeolites are among the most common minerals present in sedimentary rocks. Zeolites are found in rocks of diverse age, lithology and geological structure and are valuable indicators of sedimentation and post-deposition

* Corresponding author.
E-mail address: borodinauo@igm.nsc.ru (U. Borodina).

https://doi.org/10.1016/j.saa.2022.120979
1386-1425/

(diagenetic) setting of the host rocks [2]. The key characteristic of zeolites is framework structure with pores and interconnected voids occupied by cations and water molecules. The internal surface area of zeolite channels can reach as much as several hundred square meters per gram of zeolite, making zeolites extremely effective ion exchangers. Zeolites thus find a large number of potential applications. For instance, they can be used as carriers of molecules in order to create catalysts [3–7]. Based on clinoptilolite nanoparticles, an effective anion exchanger can be prepared [8,9]. The cation-binding physical properties of zeolites make them ideal candidates for use in the petrochemical industries and as adsorbents/exchangers for toxins, pollutants, and heavy metals [2,10]. Natural zeolites have high adsorption capacity [11–13] and are, for instance, successful adsorbents for the removal of hydrogen sulfide [12] and metallic contaminants from water [14]. Natural zeolite-bearing rocks can also be used to create simulated lunar dust [15].

The study of hydration of framework silicates during interaction with water fluid seems to be important in connection with the mechanism of conservation of partially hydrated lithosphere slab in subduction conditions. The *in situ* investigation of mineral behavior in water medium at simultaneously high *P-T* parameters can be applied to modelling mineral transformation processes in lithospheric plates [16,17]. The mineral processes in a water medium in the area of «cold» subduction, corresponding to the start of oceanic plate diving or ocean floor near geothermal sources [18,19], are of particular interest. Zeolites wairakite and phillipsite are possible participants of such slab diving [20]. Using data of 605-m layer sediments cored in Hole 841 of the Ocean Drilling Program, zeolite distribution in volcaniclastic deep-see sediments from the Tonga Trench (SW Pacific) was found [21]. It was noted that zeolites play a key role in water transport of the subducting oceanic slab. The zeolite minerals include phillipsite, clinoptilolite, analcime, mordenite, chabazite, heulandite, wairakite and erionite. This Ocean Drilling Program [21] has been proved that phillipsite is most abundant Ca-zeolite in oceanic sediments.

Wairakite $Ca[Al_2Si_4O_{12}]\cdot 2H_2O$ was first described by Steiner (1955) as the Ca-analogue of analcime $Na_2[Al_2Si_4O_{12}]\cdot 2H_2O$ [22]. It has monoclinic structure (Fig. 1a), space group *I*2/*a* (new denotation *C*2/*c*), $a = 13.692(3)$ Å, $b = 13.643(3)$ Å, $c = 13.560(3)$ Å, $\beta = 90.5(1)°$. It was first discovered from drill cores obtained from levels ranging from 600 to 2890 feets and in rocks ejected by steam from some drill holes in the Wairakei district, New Zealand. Together with analcime, pollucite, leucite, and hsianghualite, wairakite belongs to a large group of minerals with the ANA-type framework topology. It occurs widely in low-grade metamorphic rocks and hydrothermal areas [23]. The structures of the ANA-type framework topology can be synthesized using organic molecules via a multiple inorganic cation approach [24].

Wairakite decomposition and stability. Liou [25] described the dehydration of metastable disordered wairakite to metastable hexagonal anorthite, quartz and H_2O. The equilibrium of such dehydration of wairakite occurs at 330 °C at 0.05 GPa, 348 °C at 0.1 GPa, 372 °C at 0.2 GPa and 385 °C at 0.3 GPa. At lower temperatures, wairakite reacts with H_2O to form laumontite. Goryainov et al. [26] investigated the high-pressure behavior of wairakite compressed in water and glycerol up to about 10 GPa. During compression in water, two phase transitions at 1.75 and 3.10 GPa are observed. These transitions are assumed to be caused by crystal symmetry reduction in the following sequence: *C*2/*c* - $P2_1/a$ - *P*(−1) - *P*1. Ori et al. [27] investigated the elastic behavior and the high-pressure structural evolution of wairakite by means of *in situ* synchrotron X-ray powder diffraction from ambient pressure to 7.8 GPa, and upon decompression. Up to the highest investigated pressure, no complete X-ray amorphization was observed, and the original unit-cell parameters were recovered upon decompression. Still, a transition from monoclinic to a triclinic phase is observed above 2.5 GPa, with an increase of compressibility after the transition pressure. Seryotkin et al. [28] investigated the high-pressure crystal structure of wairakite by means of X-ray diffraction analysis. The heating of wairakite up to 200 °C is accompanied by a significant increase in the unit cell volume. At 145 °C, the initial monoclinic phase (*C*2/*c*) reversibly transforms into a tetragonal one ($I4_1/acd$). Upon heating above 200 °C, the dehydration of wairakite begins and is accompanied by continuous contraction with no fundamental changes in the structure while retaining symmetry $I4_1/acd$. The Ca^{2+} cations remain near the original positions, but their coordination changes from octahedral to semioctahedral.

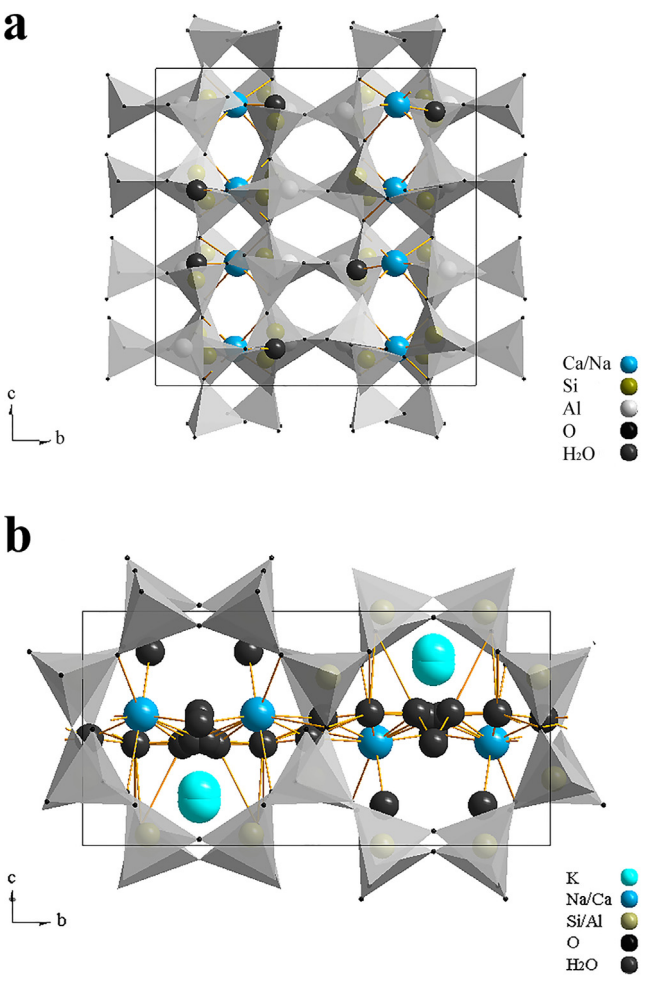

Fig. 1. The unit cell of: a – wairakite [30]; and b – phillipsite [28] as viewed from [100] plane. SiO_4/AlO_4 tetrahedra are indicated in light gray.

Phillipsite, ideal composition $K_2(Na,Ca_{0.5})_3[Al_5Si_{11}O_{32}]\cdot 12H_2O$ (Passaglia and Sheppard 2001), is very common both in sedimentary rocks and in fissures and cavities of magmatic rocks (mainly in basalts) [29] and is one of the most common natural zeolites. It has a monoclinic structure (Fig. 1b), space group $P2_1/m$, $a \approx 9.865$ Å, $b \approx 14.300$ Å, $c \approx 8.693$ Å, $\beta \approx 124.92°$ (Baerlocher et al. 2007). Phillipsites constitute a separate group of zeolites. Phillipsite Si/Al tetrahedral framework contains two main channel systems: an 8-membered ring channel along [100] and an 8-membered ring channel along [010], which intersect each other [30]. Phillipsite was first recognized in deposits on the Pacific Ocean floor by Murray and Renard in 1891 [31].

Phillipsite stability. Gatta and Lee [32] investigated phillipsite from Richmond, Victoria, Australia, with the chemical formula

$(Na_{1.64}K_{1.76}Ca_{1.19})[Al_{5.80}Si_{9.97}O_{32}]\cdot 12\cdot .47H_2O$, by *in situ* synchrotron X-ray powder diffraction up to 3.64 GPa in fluid (i.e. mix methanol: ethanol: water = 16:3:1). No phase transition was observed, but authors reported significantly anisotropic behaviour of phillipsite within the *P*-range investigated. Despite the use of a hydrous *P*-fluid, no evidence of over-hydration (by sorption of extra H_2O molecules through the eight-membered ring channels along [100] and along [010]) was observed.

Phillipsite synthesis. Park and Choi (1995) [33] described phillipsite synthesis from silica-poor fly ash by hydrothermal treatment with 2 N-NaOH solution at 105 °C. The fly ash was derived from anthracite coal and consisted of SiO_2, Al_2O_3, Fe_2O_3, Na_2O, K_2O, CaO and MgO. Park and Choi [33] concluded that phillipsite synthesis mainly depends on the Al concentration of the liquid phase and is taken place from the dissolution of the silicate glass and the amorphous Al compound. Most of the phillipsite was synthesized between 2 and 6 h. Thus, the process of the phillipsite formation could be described as follows: (1) the dissolution of amorphous materials and the condensed compound of fly ash, (2) the dissolution of the matrix of the sphere, (3) the supersaturation of liquid phase, (4) the phillipsite formation by precipitation, and (5) the growth of phillipsite crystal.

The goal of this work was *in situ* Raman investigation of wairakite and phillipsite possible non-quenchable phases and its decomposition products under simultaneously high *P-T* in a water medium (up to *P* = 3 GPa and *T* = 500 °C).

2. Material and methods

Natural samples of wairakite (Wairakei, New Zealand, space group *C*2/*c*) [28] and phillipsite (Capo di Bove, Italy) [34] were investigated. Chemical composition of these zeolites, wairakite $Ca_{0.95}Na_{0.06}[Al_{1.96}Si_{4.04}O_{12}]\cdot 2H_2O$ and phillipsite $K_2(Ca_{0.5},Na)_4[A1_{6.18}Si_{9.86}O_{32}]\cdot 12H_2O$, was determined with electron microprobe X-ray analyzer (CAMEBAX Micro, CAMECA Ltd, Japan).

In situ Raman spectra of the samples at high *P-T* conditions were recorded on a Horiba Jobin Yvon T64000 spectrometer, with resolution of 2 cm^{-1}, equipped with a liquid nitrogen cooled charge coupled device (CCD) detection system in subtractive dispersion mode at Kirensky Institute of Physics, Federal Research Center KSC SB RAS, Krasnoyarsk [35]. Ar^+ ion laser Spectra Physics Stabilite 2017 with λ = 514.5 nm and power 5 mW on a sample was used as an excitation light source. The high-pressure experiments were carried out using incident laser beam was focused on the sample by an Olympus LMPlanFl objective lens 50x (with working distance WD = 20 mm, numerical aperture N.A. = 0.35). The scattered light was collected by the same objective lens in the backscattering geometry and analyzed through a polarizer and λ-plate. Spectroscopic measurements were performed in the subtractive dispersion mode to investigate the low-wavenumber spectra, which attained a low-wavenumber limit of 8 cm^{-1} in the present setup. The deformation of the low-wavenumber spectral edge by an optical slit, which sometimes smears the true features of low-wavenumber spectra, was carefully eliminated by rigorous optical alignment.

Raman spectra of initial and *ex situ* (after high *P-T* experiments) samples were recorded with Horiba Jobin Yvon LabRam HR800 spectrometer, equipped with a 1024 pixel Peltier cooled CCD system at Sobolev Institute of Geology and Mineralogy SB RAS, Novosibirsk. A double harmonic Nd:YAG solid state laser with line of wavelength 532.1 nm and a beam power 30 mW (up to 5 mW on samples) was used as the excitation source for the analyses [36,37]. The Raman spectra were collected in a back-scattering geometry, using an Olympus BX41 microscope equipped with an Olympus objective lens 50x (with working distance WD = 0.37 mm, numerical aperture N.A. = 0.75), and a focal spot diameter of 2 μm. The spectral resolution of the recorded Stokes side of the Raman spectra was set to 2 cm^{-1} at the Raman shift of 300 cm^{-1}.

A heated high-temperature diamond anvil cell device (HT-DAC) of membrane Diacell μScope DAC HT(G) type (EasyLab, UK) with diamond IIa anvils, electrical resistive heating, water-cooling casing, and Ar gas blowing was used for Raman study of processes at simultaneously high *P* and *T*. Limiting *P-T* parameters in the working volume of the given HT-DAC are equal to 20 GPa and 800 °C. The maximal *P-T* values in the present experiments were set at 2 GPa and 400 °C for wairakite; 3 GPa and 500 °C for phillipsite. A stainless steel gasket with initial thickness of 0.25 mm is used in this DAC. Holes with a diameter of about 150-200 μm were drilled in the gaskets pre-indented to a thickness about 86 μm, for measuring at pressures up to 15 GPa. The pressure was monitored by the shift of the R_1 luminescence band of ruby [38]. The temperature was monitored using a K-type thermocouple in contact with the gasket and the diamond anvil. Water was used as a hydrostatic pressure transmission media.

Fourier transform infrared (FTIR) spectra were recorded with a Bruker IFS-113 V spectrometer in vacuum pumped chamber, using 9 mm tablets of the compressed powder sample with a binder material (polyethylene or KBr). FTIR spectra in far-infrared range of 50–400 cm^{-1} were collected using tablets with polyethylene binder. FTIR spectra in medium-infrared range of 400–4000 cm^{-1} were accumulated using tablets with KBr binder. The spectra were measured at 23 °C in transmission mode and the equipment was configured to collect a spectrum at 2 cm^{-1} resolution and 10 s collection time (10 scans co-added).

The theoretical calculations were carried out by the plane-wave pseudo-potential method based on DFT using Cambridge Serial Total Energy Package code (CASTEP) [39]. Pseudo-atom calculations were performed for O: $2s^2$, $2p^4$; Al: $3s^2$, $3p^1$; Si: $3s^2$, $3p^2$; Ca: $3s^2$, $3p^6$, $4s^2$. The structures were relaxed using the Broyden, Fletcher, Goldfarb, and Shannon (BFGS) minimization method algorithm [40]. The lattice constants and atom coordinates of the *C*2/*c* monoclinic phase of calcium wairakite were optimized, minimizing the total energy. Through a series of convergence studies concerning cut-off energies and k-points, the cut-off energies were set to 900 eV, and the ***k***-space integration over the Brillouin zone was carried out using a 1 × 1 × 1 *k*-point Monkhorst-Pack mesh [41]. These parameters were tested to ensure that the self-consistent total energies converged within 1.0×10^{-8} eV/atom. We calculated the Raman spectra using the PBE sol functional. We used the initial structural data from work [42], but excluded the water molecules from the calculations. The crystal structures of wairakite and phillipsite at atmospheric conditions (Fig. 1) were built by means of the Diamond software package [43] with cell parameters from [30] and [28].

3. Results and discussion

Raman spectra of wairakite and phillipsite under atmospheric conditions are presented in Fig. 2. Table 1 demonstrates the modes interpretation, performed according to our ab initio calculations and data from [44,45]. These data and the interpretation are in accordance with the review of Raman spectral data of zeolites [46]. Peaks of IR spectra (recorded in our laboratory, Fig. S1 and S2) and their interpretation are also presented in Table 1. Measured wairakite IR (Fig. S1) and calculated (Table S1) spectra are in accordance with IR data of wairakite at room temperature [47], where a strong change of IR spectrum at low temperature (possible phase transition) is also noted.

Raman and IR spectra (Figs. 2–3, Table 1) exhibit many peaks between 50 and 300 cm^{-1}, related to the crystal lattice vibrations

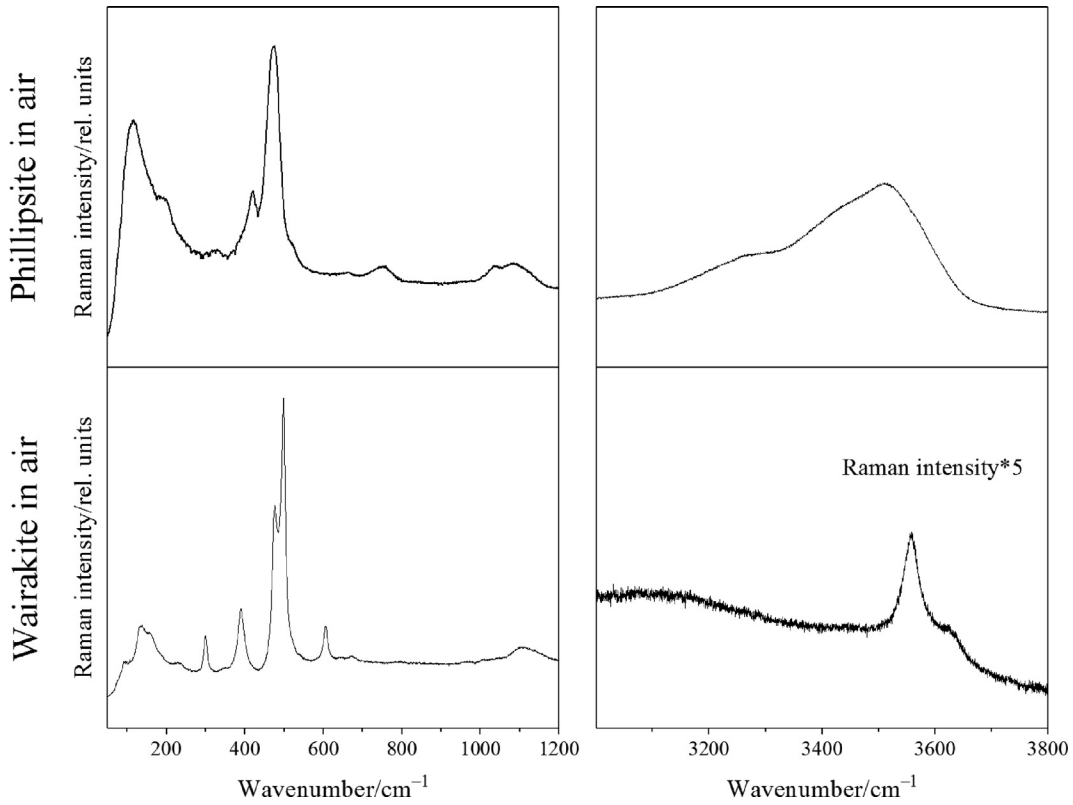

Fig. 2. Raman spectra of initial wairakite and phillipsite samples in air, presented in the ranges: 0–1200 cm^{-1}; 3000–3800 cm^{-1} (OH-stretching vibrations). The Raman scattering intensity of wairakite spectrum in the range of 3000–3800 cm^{-1} is multiplied by 5.

Table 1
Raman and IR spectra of the initial phillipsite and wairakite samples, recording at 23 °C, 1 atm, and their interpretation, performed according to our DFT calculations, which is in accordance with data [44,45]. T means tetrahedral Al and Si atoms. The interpretation represents the modes origin, however, the vibration form, the symmetry and wavenumbers differ for Raman (g-modes) and IR (u-modes) spectra. Ring breathing modes are active in Raman, but inactive in IR spectra. The breathing (breath) S4R modes involve the vibrations of four O within the ring S4R at its plane, whereas tetrahedral librations (libr TO_4) at 372 and 400 cm^{-1} involve the vibrations of O atoms in-and-out plane of the ring S6R and its deformation (def S6R).

Wavenumber, cm^{-1}				Mode interpretation
Phillipsite		Wairakite		
Raman	IR	Raman	IR	
107	113	59, 71, 73, 82, 90, 94, 99, 106, 115,	81	Lattice vibrations
166	215	122, 126, 138, 162, 174, 247, 233	114	(trans Ca,Na,K + trans TO_4 + libr TO_4)
			224	
	370	305	316	libr TO_4
		320		
	432	372	455	libr TO_4 + def S6R
		400		
418		481		bend O-T-O + breath S4R
472		504		
640	599	633	625	bend O-T-O
	678			
745	737	804	735	sym stretch T-O-T
			776	
	992	1001		sym stretch T-O
1035	1120	1134	1032	asym stretch T-O
1097			1100	
1642	1644	1622	1628	bend H-O-H
3328	3220		3492	sym stretch O-H
3509	3459	3557	3540	asym stretch O-H
		3626	3620	

that include cation translation modes (trans Ca, Na, K), translational (trans TO_4) and librational (libr TO_4) modes of TO_4 tetrahedra (T = Si, Al). The range between 300 and ~460 cm^{-1} belongs to tetrahedral librations, where the range wavenumbers are taken for wairakite (for phillipsite, there are similar, slightly shifted wavenumbers). Within this range, the subrange between 300 and ~370 cm^{-1} is assigned to predominantly librational vibrations of TO_4. The subrange between 370 and ~400 cm^{-1} is highlighted in Table 1 to show that the vibrations of interconnected tetrahedra in the crystal lead to higher wavenumbers due to the mixing

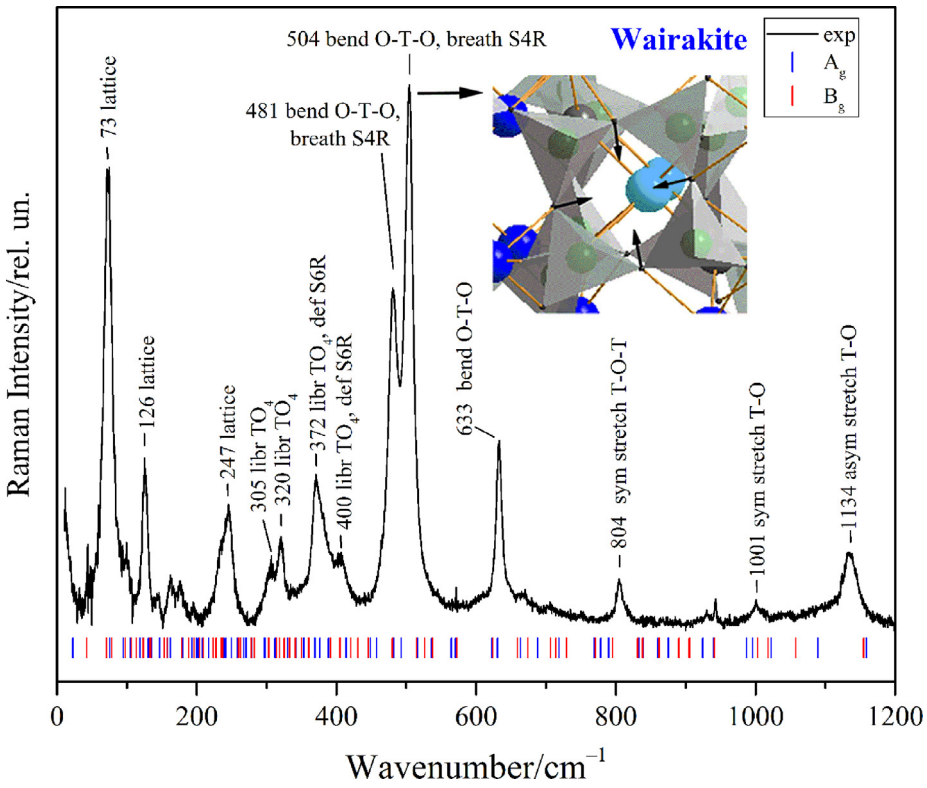

Fig. 3. Experimental (black) and calculated by DFT (color) wairakite Raman spectra. Mode interpretation was made based on DFT calculations (Table 1). The insert shows a fragment of wairakite structure in the [0 0 1] plane with 504-cm^{-1} breathing mode of S4R, involving major amplitudes of O atoms (directing with arrows).

libration-bending vibrations, where the vibration freedoms are originated from rotation motions of TO_4. These modes of medium Raman intensity also represent deformation vibrations of the single six-membered rings S6R.

Modes in the range of 460–520 cm^{-1} for wairakite (410–510 cm^{-1} for phillipsite) are related to bending O-T-O vibrations originated from E modes of 'free' tetrahedron TO_4 (T_d symmetry). Concerning vibrations in the rings formed by interconnected tetrahedra, they produce the breathing modes of single four-membered rings (S4R). These breathing S4R modes are very strong in Raman spectra of zeolites. Modes in the range of 520–680 cm^{-1} are related to the bending O-T-O vibrations originated from F_2 modes of 'free' tetrahedron TO_4. The breathing S4R modes (originated from the bending O-T-O) involves vibrations of four O within the ring S4R at its plane, whereas the bending O-T-O mode at 633 cm^{-1} involves vibrations of four O atoms and four T atoms in-and-out plane of the ring S4R.

Modes in the range of 680–810 cm^{-1} are related to symmetric stretching T-O-T vibrations of the bridge T-O-T. Modes in the 950–1020 cm^{-1} range are assigned to symmetric stretching T-O vibrations, whereas modes in the 1020–1150 cm^{-1} range are related to asymmetric stretching T-O vibrations of TO_4 tetrahedra. Weak Raman bending H-O-H vibrations are disposed at wavenumbers around 1620–1650 cm^{-1}, whereas O-H stretching vibrations are situated at wavenumbers from 3000 to 3700 cm^{-1} (Fig. 2).

We emphasize that the strongest Raman band (at 472 and 504 cm^{-1} in phillipsite and wairakite spectra, respectively) corresponds to the breathing mode of the four-membered aluminosilicate rings [45]. The interpretation of strong wairakite vibrations and the form of the strongest wairakite vibration are shown in Fig. 3. The calculated frequencies and the symmetry of some other wairakite vibrational modes (Raman active and infrared active modes) are presented in Supporting information. This interpretation of vibrational spectra of both zeolites are in good accordance with the previous interpretation and calculations carried out for other zeolites [44,45] and aluminosilicate clusters [48,49].

The *P-T* points of our experiment are indicated on the scheme of mineral equilibria (Fig. 4) corresponding to [20]. One can see that most of the experiment path lies between the stability zones of laumontite and lawsonite + quarz + fluid. The wairakite Raman spectra, recorded under various *P-T* conditions, are presented in Fig. 5. Wairakite has no polymorphic transformations during compression in water medium up to T = 250 °C and P = 0.4 GPa. At

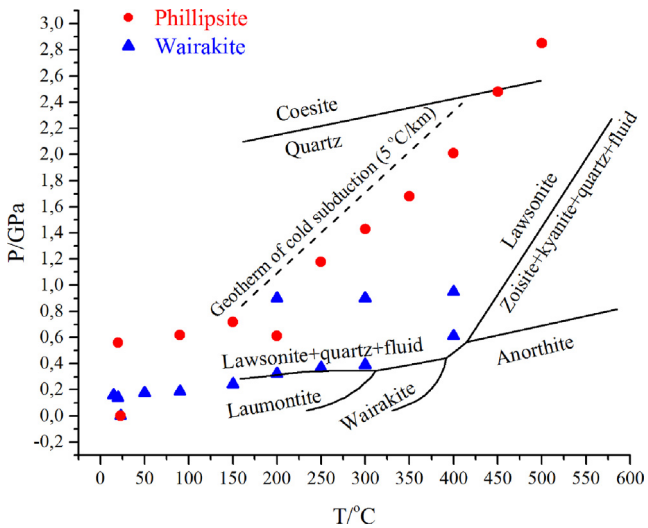

Fig. 4. *P-T* diagram of the wairakite-water system with points of our experiments with phillipsite (red circles) and wairakite (blue triangles).

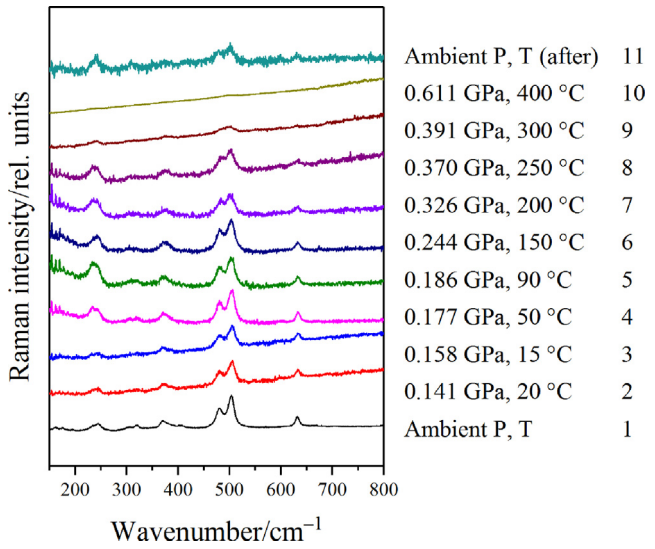

Fig. 5. Raman spectra obtained in the wairakite-water system at indicated *P-T* parameters: (1) 10^5 Pa, 23 °C – initial sample (in the air); (2–10) compressed in water media in DAC; (11) after the experiment.

higher *P-T* parameters (*T* = 250 °C and *P* = 0.4 GPa) wairakite undergoes a polymorphic transition (Fig. 5).

At *T* = 300–450 °C and *P* = 1.0 GPa, the Raman spectrum of crystal wairakite almost disappears, and in the region of ~400–600 cm^{-1} a weak halo appears, indicating amorphization, which turned out to be partially reversible. The wairakite crystals partially dissolved with a reduction of blocks by 20–40% in 4 h, as seen in the microscope (Fig. 6). Then crystals of other zeolite phillipsite grow from fluid (Fig. 7, graph.2). Its spectrum almost matches with the spectrum (Fig. 7, graph.3) of the initial phillipsite sample, used to identify the mineral.

Besides the phillipsite spectrum, among spectra obtained in the wairakite-water system after the experiment, the spectrum of unidentified phase X, exhibiting the strong doublet at 412 and 435 cm^{-1} and other bands at 116, 170, 254 and 802 cm^{-1}, was found (Fig. 7, graph. 4). The spectrum can be compared with the spectrum of Ca-chabazite (Fig. 7 graph.5) from Tablo Mountain, Baja California, Mexico (RRUFF R050014.2) and the spectrum of epistilbite (mordenite group) with a strong doublet at 410 and 438 cm^{-1} and a weak band at 804 cm^{-1} [14]. Thus, Raman spectrum of the phase X is similar to that of epistilbite or chabazite-like structure. Micro X-ray diffraction analysis needs to clarify this question. Lee at al. [14] proved that zeolite synthesis is typically multiphase, leading to simultaneously appearance of 2–3 zeolitic phases. According to [14], phillipsite can appear together with the following zeolites: ECR-1, RHO, P, L, chabazite, analcime, erionite, mordenite etc.

Though phillipsite formation (instead of lawsonite) in system wairakite-water is unexpected, it is consistent with trawling data of ocean floor, where zeolites phillipsite (Ca-Na-form) and analcime (Na-form) were found. Phillipsite crystalized in the region of the upper pressure limit of wairakite stability that is most likely due to the fast kinetics of the transition. The reaction of wairakite decomposition to lawsonite and quartz was not observed, probably due to its low kinetic ability and dissolution of wairakite because of the high content of excess water.

During compression in water with *P-T* increase, phillipsite at first does not experience polymorphic transformations (up to *T* ≈ 300 °C and *P* ≈ 1.43 GPa) (Fig. 8). At 350 °C and 1.7 GPa, the Raman bands start broadening; at 400 °C and 2 GPa, the Raman

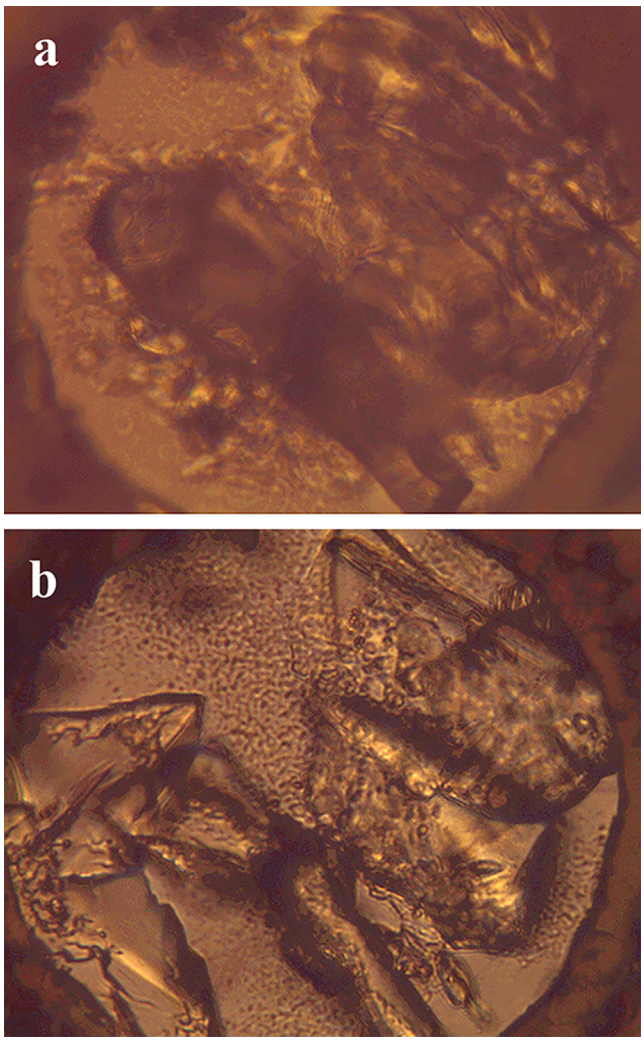

Fig. 6. Photos of the wairakite sample taken with T64000 spectrometer microscope: **a** – initial sample under atmospheric conditions; and **b** – the sample compressed at 0.95 GPa, 400 °C. Wairakite crystals are partially dissolved, and tiny crystals of phillipsite and the rounded druse of phase X are formed.

spectrum almost disappears, and in the region of ~300–600 cm^{-1} a wide halo appears, probably indicating phillipsite amorphization.

Figs. 9 and 10 represent pressure and temperature shifts of wavenumber of the strong doublet mode of wairakite (481 and 504 cm^{-1} under atmospheric conditions) and phillipsite (418 and 472 cm^{-1} under atmospheric conditions). Regular ν/*P* and ν/*T* dependencies mean positive and negative shifts, respectively. Thus, in this study, there are two competing processes affecting the value of the wavenumber, and some dependencies are not expected. In Fig. 9, one can see that the wavenumber of the wairakite peak at 481 cm^{-1} increases with both *P* and *T* increase up to approximately 0.4 GPa, 300 °C. Thus, the peak has regular pressure dependence and atypical temperature dependence. The peak at 504 cm^{-1} demonstrates opposite tendencies. Such a difference in the behavior of the modes can be explained as follows: vibrations revealed at 481 cm^{-1} and 504 cm^{-1} are related to two different four-membered rings [50,51], and one of them tapers with pressure increase, while the second expands. Peaks of the main mode of phillipsite (Fig. 10) demonstrate regular pressure dependence and then merge at approximately 1.7 GPa, 350 °C due to the band broadening. Both wairakite and phillipsite strong modes demonstrate a quite regular broadening with pressure increase.

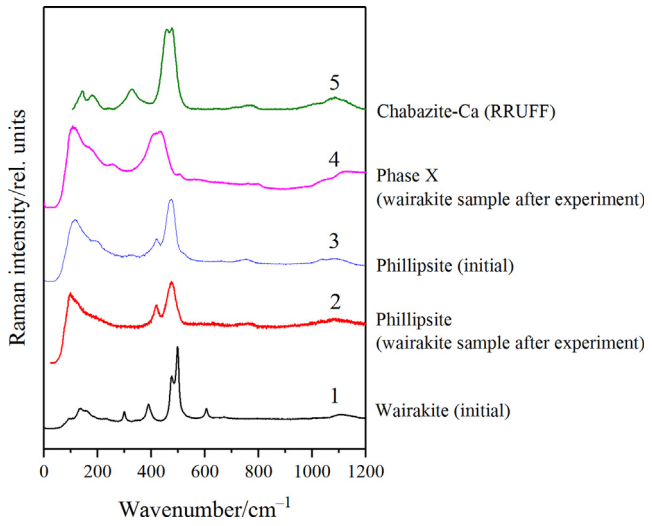

Fig. 7. Raman spectra: graph.1- initial sample of wairakite; graph.2 - phillipsite obtained from the wairakite sample during the experiment; graph.3 - spectrum of initial phillipsite sample; graph.4 - spectrum of unidentified phase X obtained from the wairakite sample during the experiment; graph.5 - spectrum of Ca-chabazite from Tablo Mountain, Baja California, Mexico (RRUFF R050014.2).

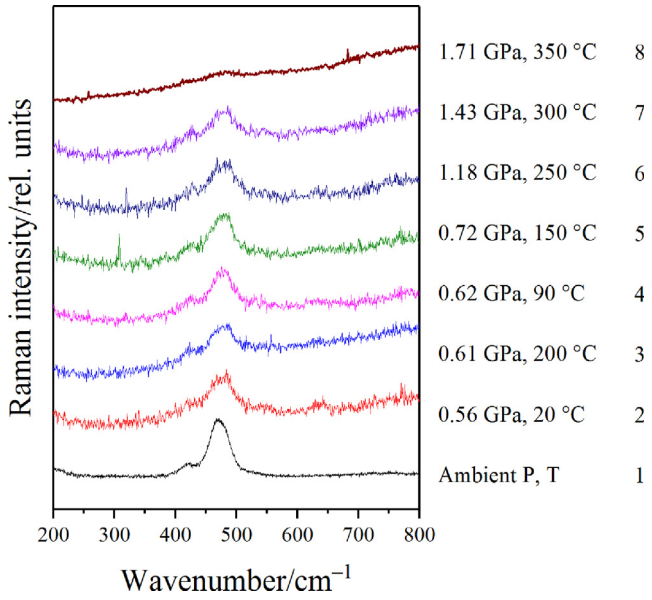

Fig. 8. Raman spectra obtained in phillipsite-water system at indicated *P-T* parameters: (1) 10^5 Pa, 23 °C – initial sample (in air); (2–8) compressed in water medium in DAC.

In this way, phillipsite compressed in a water medium does not undergo polymorphic transformation at the *P-T* parameters used in this study. At maximal *P-T* parameters, 2.85 GPa and 500 °C, phillipsite completely dissolves and probably decomposes, but no decomposition products in crystalline form are observed. Wairakite compressed in a water medium does not experience polymorphic transformation up to 0.4 GPa, 250 °C. Raman spectra demonstrate that wairakite has a polymorphic transformation at $P \approx 0.4$ GPa and $T \approx 300$ °C. During further *P-T* increase, its Raman spectrum almost disappears, wairakite dissolves, and another zeolite phillipsite grows from aqueous solution. The *in situ* observed phillipsite formation from wairakite at *P-T* parameters in the range of the upper-pressure limit of wairakite stability may explain very rare abundance (or absence in some samples) of wairakite and the widespread occurrence of phillipsite in marine sediments (data of [21]).

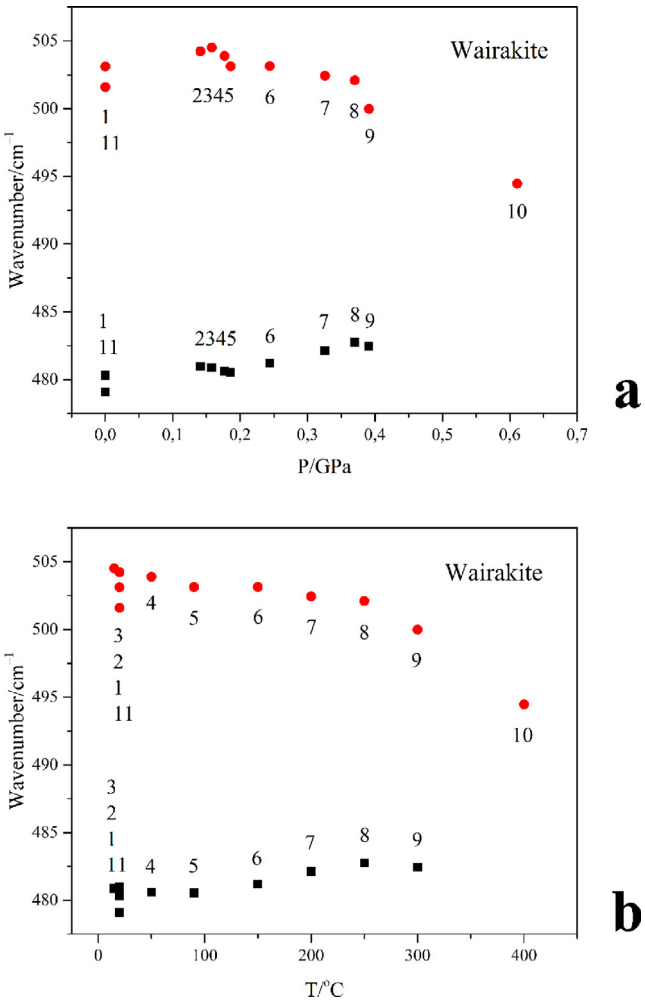

Fig. 9. *v*/*P* (**a**) and *v*/*T* (**b**) dependencies of the intense doublet mode of wairakite (481 and 504 cm^{-1} under atmospheric conditions). Numbers of *P-T* points correspond to the numbers in Fig. 5.

4. Conclusion

Raman and FTIR transmission spectra of wairakite and phillipsite were recorded and interpreted. Based on ab initio DFT calculations of wairakite, an interpretation of the Raman and IR spectra of both zeolites is presented. All observed peaks of the vibrational spectra were successfully assigned to certain vibrations. The strongest Raman bands of both zeolites are related to the breathing modes of single four-membered aluminosilicate rings S4R, originated from O-T-O bending vibrations in interconnected tetrahedral TO_4 groups. This interpretation of vibrational spectra of both zeolites is in accordance with the previous interpretation and calculations carried out for other zeolites [44,45] and aluminosilicate clusters [48,49].

Phillipsite compressed in water retains the initial phase up to the upper limit of the *P-T* parameters studied. Wairakite compressed in water exhibits one polymorphic transition at $T \approx 300$ °C and $P \approx 0.4$ GPa. At 300–450 °C and $P = 1$ GPa Raman spectrum nearly disappears due to the amorphization of wairakite. Wairakite crystals partially dissolve with further formation of zeolite phillipsite from the fluid at $T > 250$ °C and $P > 0.4$ GPa. Phillipsite crystallizes in the region of the upper pressure stability limit of

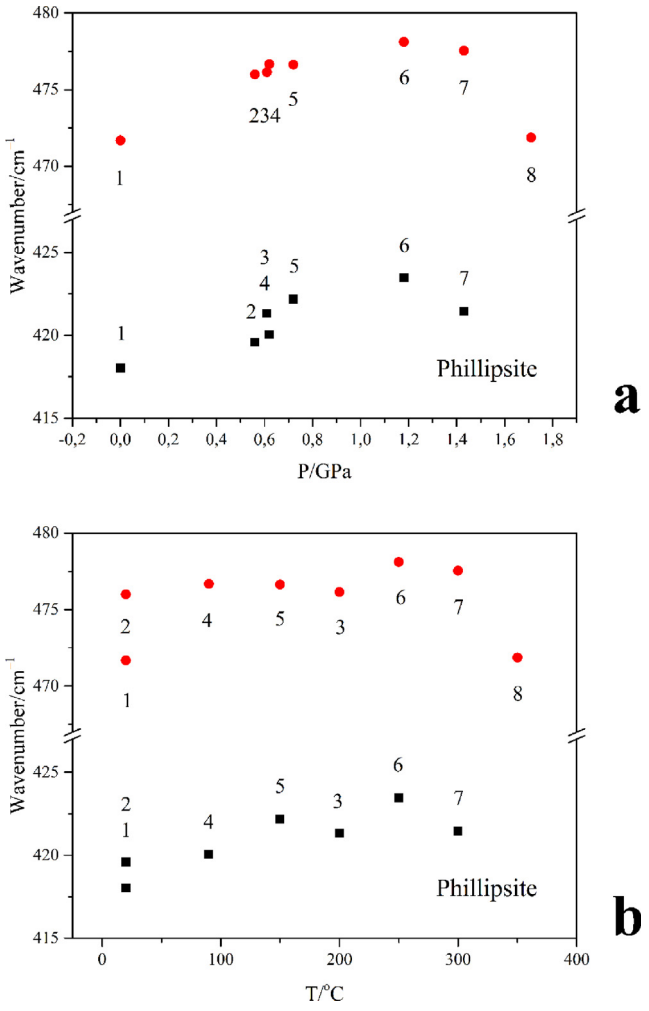

Fig. 10. v/P (**a**) and v/T (**b**) dependencies of the intense doublet mode of phillipsite (418 and 472 cm^{-1} under atmospheric conditions). Numbers of *P-T* points correspond to the numbers in Fig. 8.

wairakite, which is probably due to the rapid kinetics of this transition. Moreover, we observe multiple formation of zeolites from wairakite: phillipsite and phase X that is chabazite-like zeolite or epistilbite. The reaction leading to lawsonite and quartz formation is not observed, probably due to its low kinetic ability and water excess in the system.

Phillipsite probably crystallizes from ocean salts, including zeolitic rocks, under moderate *P-T* conditions. Phillipsite during our experiments was stable at similar *P-T* conditions up to its dissolution in water fluid. Based on these investigation results, we can suggest greater phillipsite *P-T* stability in lithospheric plates compared to wairakite of analcime group. Thus, our *in situ* observation of the transformation of wairakite to phillipsite (as the dominant product of decomposition) and the *P-T* testing of phillipsite stability may be experimental evidence that, among Ca-zeolites, phillipsite is the most stable phase in oceanic sediments, which is consistent with the investigations carried out during Ocean Drilling Program [21].

Declaration of Competing Interest

The authors declare that they have no known competing financial interests or personal relationships that could have appeared to influence the work reported in this paper.

Acknowledgements

This work was performed under the auspicious of the state assignment of the Sobolev Institute of Geology and Mineralogy SB RAS, Kirensky Institute of Physics, Federal Research Center KSC SB RAS. Krasnoyarsk Regional Center of Research Equipment of Federal Research Center «Krasnoyarsk Science Center SB RAS» was used for the Raman experiment.

Appendix A. Supplementary material

Supplementary data to this article can be found online at https://doi.org/10.1016/j.saa.2022.120979.

References

[1] G. Gottardi, E. Galli, Natural Zeolites, 18, Springer Science & Business Media, 2012.
[2] K. Ramesh, D.D. Reddy, Zeolites and their potential uses in agriculture, Adv. Agron. 113 (2011) 219–241.
[3] A. Pourtaheri, A. Nezamzadeh-Ejhieh, Enhancement in photocatalytic activity of NiO by supporting onto an Iranian clinoptilolite nano-particles of aqueous solution of cefuroxime pharmaceutical capsule, Spectrochim. Acta Part A: Mol. Biomol. Spectrosc. 137 (2015) 338–344.
[4] F. Iazdani, A. Nezamzadeh-Ejhieh, Supported cuprous oxide-clinoptilolite nanoparticles: Brief identification and the catalytic kinetics in the photodegradation of dichloroaniline, Spectrochim. Acta Part A Mol. Biomol. Spectrosc. 250 (2021) 119348.
[5] F. Iazdani, A. Nezamzadeh-Ejhieh, Photocatalytic kinetics of 2, 4-dichloroaniline degradation by NiO-clinoptilolite nanoparticles, Spectrochim. Acta Part A Mol. Biomol. Spectrosc. 250 (2021) 119228.
[6] A. Nezamzadeh-Ejhieh, Z. Ghanbari-Mobarakeh, Heterogeneous photodegradation of 2, 4-dichlorophenol using FeO doped onto nano-particles of zeolite P, J. Ind. Eng. Chem. 21 (2015) 668–676.
[7] A.N. Ejhieh, M. Khorsandi, Photodecolorization of Eriochrome Black T using NiS–P zeolite as a heterogeneous catalyst, J. Hazard. Mater. 176 (1–3) (2010) 629–637.
[8] T. Tamiji, A. Nezamzadeh-Ejhieh, Sensitive voltammetric determination of bromate by using ion-exchange property of a Sn(II)-clinoptilolite-modified carbon paste electrode, J. Solid State Electrochem. 23 (1) (2019) 143–157.
[9] A. Nezamzadeh-Ejhieh, M. Shahanshahi, Modification of clinoptilolite nano-particles with hexadecylpyridynium bromide surfactant as an active component of Cr (VI) selective electrode, J. Ind. Eng. Chem. 19 (6) (2013) 2026–2033.
[10] G. Reid, S. Klebe, N. van Zandwijk, A.M. George, Asbestos and Zeolites: from A to Z via a Common Ion, Chem. Res. Toxicol. 34 (4) (2021) 936–951.
[11] S. Wang, Y. Peng, Natural zeolites as effective adsorbents in water and wastewater treatment, Chem. Eng. J. 156 (1) (2010) 11–24.
[12] M. Ozekmekci, G. Salkic, M.F. Fellah, Use of zeolites for the removal of H2S: a mini-review, Fuel Process. Technol. 139 (2015) 49–60.
[13] S. Wang, K. Hou, H. Heinz, Accurate and compatible force fields for molecular oxygen, nitrogen, and hydrogen to simulate gases, electrolytes, and heterogeneous interfaces, J. Chem. Theory Comput. 17 (8) (2021) 5198–5213.
[14] L.C. Oliveira, D.I. Petkowicz, A. Smaniotto, S.B. Pergher, Magnetic zeolites: a new adsorbent for removal of metallic contaminants from water, Water Res. 38 (17) (2004) 3699–3704.
[15] M. Manzoli, O. Tammaro, A. Marocco, B. Bonelli, G. Barrera, P. Tiberto, S. Esposito, New insights in the production of simulated moon agglutinates: the use of natural zeolite-bearing rocks, ACS Earth Space Chem. (2021).
[16] U. Borodina, A. Likhacheva, A. Golovin, S. Goryainov, S. Rashchenko, Raman spectra of shortite $Na_2Ca_2(CO_3)_3$ compressed up to 8 GPa, High Pressure Res. 38 (3) (2018) 293–302.
[17] U. Borodina, S. Goryainov, A. Oreshonkov, A. Shatskiy, S. Rashchenko, Raman study of 3.65 Å-phase $MgSi(OH)_6$ under high pressure and the bands assignment, High Pressure Res. 40 (4) (2020) 495–510.
[18] A.R. Pawley, N.J. Chinnery, S.M. Clark, M.J. Walter, Experimental study of the dehydration of 10-Aa phase, with implications for its H2O content and stability in subducted lithosphere, Contrib. Miner. Petrol. 162 (6) (2011) 1279–1289.
[19] L.H. Rüpke, J.P. Morgan, M. Hort, J.A. Connolly, Serpentine and the subduction zone water cycle, Earth Planet. Sci. Lett. 223 (1–2) (2004) 17–34.
[20] S. Rashchenko, A.Y. Likhacheva, A.D. Chanyshev, A.I. Ancharov, The application of in situ X-ray diffraction for the study of mineral reactions: The formation of lawsonite at 400° C and 25 kbar, J. Struct. Chem. 53 (1) (2012) 43–46.
[21] F. Vitali, G. Blanc, P. Larque, Zeolite distribution in volcaniclastic deep-sea sediments from the Tonga Trench margin (SW Pacific), Clays Clay Miner. 43 (1) (1995) 92–104.
[22] A. Steiner, Wairakite, the calcium analogue of analcime a new zeolite mineral, Batey, 1955.
[23] G. Gottardi, E. Galli, Zeolites of the heulandite group, in: Natural Zeolites, Springer, 1985, pp. 256–305.

[24] H. Lee, J. Shin, S.B. Hong, Tetraethylammonium-mediated zeolite synthesis via a multiple inorganic cation approach, ACS Mater. Lett. 3 (4) (2021) 308–312.
[25] J. Liou, Synthesis and stability relations of wairakite, $CaAl_2Si_4O_{12}{\cdot}2H_2O$, Contrib. Miner. Petrol. 27 (4) (1970) 259–282.
[26] S. Goryalnov, B. Fursenko, I. Belitskil, Raman spectroscopy of phase transitions and amorphization of wairakite at high pressures, Doklady Physical Chemistry, Pleiades Publishing, Ltd., 1999.
[27] S. Ori, S. Quartieri, G. Vezzalini, V. Dmitriev, Pressure-induced structural deformation and elastic behavior of wairakite, Am. Mineral. 93 (1) (2008) 53–62.
[28] Y.V. Seryotkin, W. Joswig, V.V. Bakakin, I.A. Belitsky, B.A. Fursenko, High-temperature crystal structure of wairakite, Eur. J. Mineral. 15 (3) (2003) 475–484.
[29] E. Galli, A.G. Loschi Ghittoni, The crystal chemistry of phillipsites, Am. Mineral.: J. Earth Planet. Mater. 57 (7–8) (1972) 1125–1145.
[30] G.D. Gatta, P. Cappelletti, N. Rotiroti, C. Slebodnick, R. Rinaldi, New insights into the crystal structure and crystal chemistry of the zeolite phillipsite, Am. Mineral. 94 (1) (2009) 190–199.
[31] J. Murray, A.F. Renard, Report on deep-sea deposits based on the specimens collected during the voyage of HMS Challenger in the years 1872 to 1876, HM Stationery Office, 1891.
[32] G.D. Gatta, Y. Lee, Anisotropic elastic behaviour and structural evolution of zeolite phillipsite at high pressure: A synchrotron powder diffraction study, Microporous Mesoporous Mater. 105 (3) (2007) 239–250.
[33] M. Park, J. Choi, Synthesis of phillipsite from fly ash, Clay Sci. 9 (4) (1995) 219–229.
[34] W. Mozgawa, The relation between structure and vibrational spectra of natural zeolites, J. Mol. Struct. 596 (1–3) (2001) 129–137.
[35] S.V. Goryainov, S.N. Krylova, U.O. Borodina, A.S. Krylov, Dynamical immiscibility of aqueous carbonate fluid in the Shortite-Water system at high-pressure–temperature conditions, J. Phys. Chem. C 125 (33) (2021) 18501–18509.
[36] S. Goryainov, Y. Pan, M.B. Smirnov, W. Sun, J.X. Mi, Raman investigation on the behavior of parasibirskite $CaHBO_3$ at high pressure, Spectrochim. Acta Part A Mol. Biomol. Spectrosc. 173 (2017) 46–52.
[37] S. Grishina, S. Goryainov, A. Oreshonkov, N. Karmanov, Micro-Raman study of cesanite ($Ca_2Na_3(OH)(SO_4)_3$) in chloride segregations from Udachnaya-East kimberlites, J. Raman Spectrosc. (2021).
[38] F. Datchi, A. Dewaele, P. Loubeyre, R. Letoullec, Y. Le Godec, B. Canny, Optical pressure sensors for high-pressure–high-temperature studies in a diamond anvil cell, High Pressure Res. 27 (4) (2007) 447–463.
[39] S.J. Clark, M.D. Segall, C.J. Pickard, P.J. Hasnip, M.I. Probert, K. Refson, M.C. Payne, First principles methods using CASTEP, Zeitschrift für Kristallographie-Crystall. Mater. 220 (5–6) (2005) 567–570.
[40] B.G. Pfrommer, M. Côté, S.G. Louie, M.L. Cohen, Relaxation of crystals with the quasi-Newton method, J. Comput. Phys. 131 (1) (1997) 233–240.
[41] H.J. Monkhorst, J.D. Pack, Special points for Brillouin-zone integrations, Phys. Rev. B 13 (12) (1976) 5188.
[42] C.M.B. Henderson, A.M.T. Bell, S.C. Kohn, C.S. Page, Leucite-pollucite structure-type variability and the structure of a synthetic end-member calcium wairakite ($CaAl_2Si_4O_{12}{\cdot}2H_2O$), Mineral. Mag. 62 (2) (1998) 165–178.
[43] K. Brandenburg, H. Putz, Diamond-crystal and molecular structure visualization crystal impact, Rathausgasse 30 (1999) 1997–2000.
[44] F. Pechar, Study of the Raman polarization spectra of the single crystal phillipsite, Kristall und Technik 16 (8) (1981) 917–920.
[45] S.V. Goryainov, M.B. Smirnov, Raman spectra and lattice-dynamical calculations of natrolite, Eur. J. Mineral. 13 (3) (2001) 507–519.
[46] Y.-L. Tsai, E. Huang, Y.H. Li, H.T. Hung, J.H. Jiang, T.C. Liu, H.F. Chen, Raman spectroscopic characteristics of zeolite group minerals, Minerals 11 (2) (2021) 167.
[47] S. Goryainov, B. Fursenko, I. Belitsky, Phase transitions in analcime and wairakite at low-high temperatures and high pressure, Phys. Chem. Miner. 23 (4) (1996) 297–298.
[48] W. Mozgawa, M. Handke, W. Jastrzębski, Vibrational spectra of aluminosilicate structural clusters, J. Mol. Struct. 704 (1–3) (2004) 247–257.
[49] K.A. Iyer, S.J. Singer, Local-mode analysis of complex zeolite vibrations: Sodalite, J. Phys. Chem. 98 (48) (1994) 12670–12678.
[50] Y.M. Miroshnichenko, S. Goryainov, Raman study of high-pressure phase transitions in dehydrated analcime, Mineral. Mag. 64 (2) (2000) 301–309.
[51] G.D. Gatta, F. Nestola, T.B. Ballaran, Elastic behavior, phase transition, and pressure induced structural evolution of analcime, Am. Mineral. 91 (4) (2006) 568–578.